ELSEVIER

International Journal of Mass Spectrometry 218 (2002) 181–196

International Journal of Mass Spectrometry

www.elsevier.com/locate/ijms

Transition curves and *iso*-β_u lines in nonlinear Paul traps

S. Sevugarajan, A.G. Menon*

Department of Instrumentation, Indian Institute of Science, Bangalore 560012, India

Received 27 February 2002; accepted 30 April 2002

Abstract

This paper has the motivation to understand the role of field inhomogeneties in altering stability boundaries in nonlinear Paul traps mass spectrometers. With the inclusion of higher order terms in the equation of motion, the governing equation takes the form of a nonlinear Mathieu equation. The harmonic balance technique has been used to obtain periodic solutions which represents the transition curves, $\beta_u = 0$ and $\beta_u = 1$. A continuous fraction expression, similar in form to the linear case, has also been derived to plot *iso*-β_u lines within the stability region. The expression qualitatively reflects experimental observations in literature related to ion stabilities in nonlinear traps. The role of hexapole and octopole superposition in shifting the stable region as well as ion secular frequencies in nonlinear Paul traps has been discussed using the analytical expression derived in this paper. (Int J Mass Spectrom 218 (2002) 181–196)

Keywords: Nonlinear Paul traps; Nonlinear Mathieu equation; Harmonic balance method; Transition curves and *iso*-β_u lines

1. Introduction

The Paul trap mass spectrometer consists of a three electrode geometry mass analyzer with two endcap electrodes and a central ring electrode, all machined to a hyperboloid geometry [1,2]. Ions of an analyte gas are trapped in the central cavity of the mass analyzer when an oscillating rf potential is applied between the central ring electrode and the endcap electrodes [1,3,4]. In an ideal Paul trap mass spectrometer, the equations of motion of the ion in the axial and radial direction are uncoupled, and can be written in the canonical form of the linear Mathieu equation [5,6]

$$\ddot{u} + (a_u + 2q_u \cos 2\xi)u = 0 \tag{1}$$

where u represents the position co-ordinates in the r and z direction and

$$\xi = \tfrac{1}{2}\Omega t \tag{2}$$

$$a_z = -2a_r = -\frac{8eU_0}{mr_0^2\Omega^2} \tag{3}$$

$$q_z = -2q_r = -\frac{4eV_0}{mr_0^2\Omega^2} \tag{4}$$

where t is time, e charge of an electron, m the mass of ion, U_0 the magnitude of the dc potential, V_0 the magnitude of the rf potential (zero-peak), Ω the angular frequency of the rf potential and r_0 is the radius of the central ring electrode.

Stability of ions in Paul traps is characterized by the overlap region (on an a–q plot) where both the axial and radial motions are stable. Within this region, ions execute motion with characteristic frequencies, referred to as the ion's secular frequency, which depends on the operating parameters of the trap. The secular frequency of the ion is given by the expression

* Corresponding author. E-mail: agmenon@isu.iisc.ernet.in

1387-3806/02/$ – see front matter
PII S1387-3806(02)00692-9

$$\omega_{\text{secular}} = \tfrac{1}{2}\beta_u \Omega \quad (5)$$

where β_u is a parameter dependent on the Mathieu parameters a and q, through a continuous fraction relationship [3,7]. The stability boundaries on the Mathieu stability plot, corresponding to periodic solution of Eq. (1), are marked by the curves of β_z and β_r having values of 0 and 1. The lines corresponding to fractional β_z or β_r values, called the *iso*-β_u lines, can be traced inside the Mathieu plot by using the continuous fraction relationship.

Over the past several years reports in literature suggest that in practical Paul traps both the stability boundary as well as the secular frequencies are different from those predicted by the Mathieu equation. The shift of stability boundaries in nonlinear ion traps due to the hexapole and octopole superposition has been discussed by Franzen [8]. Perturbation in stability diagram due to space charge has been observed by Fischer [9], Dawson [1] and Fulford et al. [10] in a three-dimensional quadrupole ion trap. Johnson et al. [11] have made a comparative study of the Mathieu stability plot between a linear and a stretched quadrupole ion trap. Arkin et al. [12] in their characterization studies of a hybrid trap have observed shift in stability boundaries in z and r directions. Franzen [13] and Franzen et al. [14] in their simulation studies have observed shifts in secular frequencies due to hexapole and octopole superpositions. Makarov [15] and Luo et al. [16] using a Duffing oscillator [17–19] model have discussed the shift in secular frequencies due to the higher order multipole superpositions. Sugiyama and Yoda [20] have experimentally observed perturbation in ion secular frequencies in their studies on anharmonic oscillations of ions trapped in a rf trap with light buffer gas. Cox et al. [21] have experimentally investigated mass shifts in nonlinear ion traps. Secular frequency shifts have also been observed by Nappi et al. [22] by using non-destructive ion detection method.

The hardware configuration of the practical Paul trap differs from the ideal Paul trap in that the practical traps have truncated electrodes [23], holes in one endcap electrode for enabling entry of electrons for ionization of the analyte gas and holes in the other endcap electrode for collection of destabilized ions, mechanical misalignment in addition to experimental constraints such as space charge [24], damping due to the buffer gas [25] and excitation potential applied to the endcap electrodes [26,27]. An important consequence of the practical and experimental constraints is that the field inside the trap is no longer linear but has small multipole contributions. These multipole terms in the potential function results in the equation of motion taking the form of a nonlinear Mathieu equation with appropriately weighted higher order terms appearing in the Mathieu equation.

In ion traps, the influence of multipole field superpositions on ion dynamics has been exhaustively, numerically, investigated by Franzen et al. [14] and the role of the different higher order field terms on ion motion at $q_{\text{cut-off}}$ has been discussed. There are now simulation packages available which simulate ion trajectories in nonlinear fields. Examples of such packages include the integrated system for ion simulation (ISIS) program by Londry et al. [28], simulation program for quadrupole resonance (SPQR) by March and co-workers [26,27], the ITSIM of Bui and Cooks [29] and Dahl's SIMION [30]. Analytically, attempts to understand ion dynamics in practical Paul traps have relied on the solution of the Duffing equation. Examples of the use of Duffing equation in practical Paul traps to understand ion dynamics include the report of Makarov [15], Luo et al. [16], Vedel et al. [31], Sugiyama and Yoda [25] and a few efforts by our group [32–34]. The limitation of the Duffing equation in the context of our present effort is primarily on account of its applicability to q values of up to about 0.4. Beyond this q-value, the assumption that the amplitude of the micromotion is small in comparison to the secular motion no longer holds. In a recent study, however, along the $a = 0$ axis at $\beta_z = 1$, Sudakov [35] has successfully used the Duffing equation to model the beat envelop at the stability boundary as a slow variable but this may not be possible along the entire perimeter of the stability boundary.

In the linear Mathieu equation, at the stability boundary, there is both a periodic solution as well as

one whose amplitude grows linearly with time. Therefore, finding a periodic solution is exactly equivalent to finding the stability boundary. However, for the nonlinear equation this is not so. As shown for the $\beta_z = 1$ line by Sudakov [35], as the rf is slowly ramped and the stability boundary is crossed, the "periodic solution" manifests as an oscillatory solution with a slowly growing amplitude. When the amplitude becomes sufficiently large the ion is detected. It has been recognized that the presence of multipole fields "blurs" the sharpness of the stability boundaries and both experimental [11,12,36] and simulation studies [8,35] have referred to early and delayed ejection of ions at the stability boundary being caused by field inhomogeneties. It was seen that positive octopole superposition causes an early ejection where as negative octopole and hexapole superposition results in delayed ejection. This lack of sharpness of the stability boundary arises on account of transition curve having amplitude dependence [35].

In this paper, we examine the transition curves obtained by assuming a periodic solution to a weakly nonlinear Mathieu equation to define the $\beta_u = 0$ and $\beta_u = 1$ boundaries. It will be seen that the transition curves we present for small nonlinearities, as is the case in practical traps, does explain the influence of higher order superpositions reported in literature. Additionally, an emphasis will be on developing a continuous fraction relationship for β_u, as is available for the linear Mathieu equation, to enable construction of *iso*-β_u lines, which in turn provides a means to estimate secular frequencies throughout the stability region in nonlinear Paul traps.

2. Equation of ion motion in nonlinear fields

The ion motion inside the trap can be obtained from its Lagrangian L [37,38], which is given by

$$L = \tfrac{1}{2}m(\dot{z}^2 + \dot{r}^2) - eV(r, z, t) \tag{6}$$

where m is the mass of the ion, $V(r, z, t)$ is the potential distribution function, $\dot{z}$ and $\dot{r}$ corresponds to the velocities in axial and radial directions, respectively. The corresponding equation of motion of the system is given by

$$\frac{\mathrm{d}}{\mathrm{d}t}\left(\frac{\partial L}{\partial \dot{u}}\right) - \frac{\partial L}{\partial u} = 0 \tag{7}$$

Here u corresponds to the generalized co-ordinates in axial (z) and radial (r) directions, respectively. The potential distribution within the ideal Paul trap has both spherical and rotational symmetry. In a practical ion trap where nonlinearities are present, Legendre polynomials are normally selected for expressing these nonlinearities [38–40] since it has the same symmetry as the system for representing the higher order terms.

If P_n is the Legendre polynomial of order n, then the potential distribution inside the trap in terms of spherical coordinates (ρ, θ, φ) is given by

$$\phi(\rho, \theta, \varphi) = \phi_0 \sum_{n=0}^{\infty} A_n \frac{\rho^n}{r_0^n} P_n(\cos\theta) \tag{8}$$

where A_n is the dimensionless weight factors for different multipole terms, ρ is the position vector and ϕ_0 is a time-dependent quantity and is given by

$$\phi_0 = U_0 + V_0 \cos \Omega t \tag{9}$$

In our computations two higher order multipoles viz., hexapole and octopole superpositions corresponding to $n = 3$ and 4, are taken into account along with the quadrupole component for calculating the potential distribution inside the trap. Expanding Eq. (8) by substituting the Legendre polynomials used by Beaty [39] for representing the higher order multipoles, we get the following expression for the potential distribution inside the trap as

$$\begin{aligned} V(z, r, t) = &-\frac{A_2}{r_0^2}(U_0 + V_0 \cos \Omega t) \\ &\times \left[z^2 - \frac{r^2}{2} + \frac{h}{r_0}\left(z^3 - \frac{3}{2}zr^2\right)\right. \\ &\left. + \frac{f}{r_0^2}\left(z^4 - 3r^2z^2 + \frac{3}{8}r^4\right)\right] \end{aligned} \tag{10}$$

where $h = A_3/A_2$ and $f = A_4/A_2$ and A_2, A_3 and A_4 are the strength of quadrupole, hexapole and octopole superposition, respectively. In ideal Paul traps

the weight factor $A_2 = 1$ and weight factors of higher order multipole (in our computations A_3 and A_4) are zero. In nonlinear traps, the boundary conditions ($r = r_0$ and $z = 0$) and ($r = 0$ and $z = z_0$) can be used to obtain the value of the quadrupole weight factor. For a trap with hexapole and octopole superpositions with a potential ϕ_0 being applied to the central ring electrode and with the endcap electrodes kept at ground potential we have

$$A_2 \cong \left[1 - \tfrac{1}{2\sqrt{2}}h + \tfrac{1}{8}f\right] \tag{11}$$

In the axial direction for deriving the equation of ion motion from Eq. (6) we have

$$\frac{\partial L}{\partial \dot{z}} = m\dot{z} \tag{12}$$

$$\frac{\partial L}{\partial z} = \frac{eA_2}{r_0^0}(U_0 V \cos \Omega t) \times \left[2z + \frac{h}{r_0}\left(3z^2 + \frac{3}{2}r^2\right) + \frac{f}{r_0^2}(4z^3 - 6r^2 z)\right] \tag{13}$$

Although coupled secular oscillations have been reported in experimental literature [31], from the point of view of simplicity of our analysis we have neglected coupled oscillations. With this approximation, the axial and radial motion can be written as a pair of uncoupled equations by neglecting the terms involving r in axial direction and by neglecting the terms involving z in the radial direction. The equation of ion motion in axial direction is obtained by substituting Eqs. (12) and (13) in Eq. (7) and by introducing the transformation $\xi = \frac{\Omega t}{2}$, we get

$$\ddot{z} - \frac{8eA_2}{mr_0^2\Omega^2}(U_0 + V_0 \cos 2\xi) \times \left(z + \frac{3h}{2r_0}z^2 + \frac{2f}{r_0^2}z^3\right) = 0 \tag{14}$$

Eq. (14) can be rewritten as

$$\ddot{z} + (a_z + 2q_z \cos 2\xi)(z + \alpha_{2z}z^2 + \alpha_{3z}z^3) = 0 \tag{15}$$

where $\ddot{z}$ corresponds to the second derivative with respect to ξ and

$$a_z = -\frac{8eA_2U_0}{mr_0^2\Omega^2} \tag{16}$$

$$q_z = -\frac{4eA_2V_0}{mr_0^2\Omega^2} \tag{17}$$

$$\alpha_{2z} = \frac{3h}{2r_0} \tag{18}$$

$$\alpha_{3z} = \frac{2f}{r_0^2} \tag{19}$$

Equation of ion motion in radial direction can be similarly obtained, and is given by

$$\ddot{r} + (a_r + 2q_r \cos 2\xi)(r + \alpha_{3r}r^3) = 0 \tag{20}$$

where

$$a_r = \frac{4eA_2U_0}{mr_0^2\Omega^2} \tag{21}$$

$$q_r = \frac{2eA_2V_0}{mr_0^2\Omega^2} \tag{22}$$

$$\alpha_{3r} = -\frac{3f}{2r_0^2} \tag{23}$$

Eqs. (16), (17), (21) and (22) are expressions for computing the Mathieu parameters in the axial and radial directions. Eqs. (15) and (20) represent the equation of ion motion in axial and radial directions, respectively when there is hexapole and octopole superposition. The nonlinear quadratic and cubic terms that appears in the second bracket in Eq. (15) represents the field nonlinearity created by hexapole and octopole superposition in axial direction. The coefficients α_{2z} and α_{3z}, which in turn are related to h and f, incorporate the magnitudes of the hexapole and octopole superpositions, respectively. With reference to the radial equation of motion, the cubic term in Eq. (20) represents the field nonlinearity due to octopole superposition in radial direction and α_{3r}, which is related to f, is the magnitude of the octopole superposition in radial direction. It should be noted that for a particular hexapole and octopole superposition, motion of ions are affected in axial direction due to both hexapole and octopole superpositions whereas in radial direction hexapole superposition does not have any effect

on ion motion. This is seen by the absence of hexapole term in the equation of ion motion in radial direction.

3. Transition curves in nonlinear Paul traps

In mathematical literature stability of the nonlinear Mathieu equation of the form

$$\ddot{z} + (a_z - 2q_z \cos 2\xi)z \pm kz^3 = 0 \tag{24}$$

has received attention for their importance in mechanical systems. Stability and the periodic solutions to equations of the form given by Eq. (24) have been investigated by McLachlan [41] and Mahmoud [42] using harmonic balance and generalized averaging method, respectively. Hsieh [43] also investigated the stability of Eq. (24) with an additional damping term by taking a asymptotic trial solution. Zavodney and Nayfeh [44] investigated Eq. (24) with additional damping and quadratic nonlinear term in their studies on single degree of freedom system with quadratic and cubic nonlinearities to a fundamental parametric resonance. Natsiavas et al. [45] have investigated the equation similar to Eq. (15) without quadratic nonlinearity but with damping subjected to an external excitation by using multiple scales method. The difference between Eqs. (15) and (24) is the way in which the nonlinear terms are added to the linear Mathieu equation. The nonlinear terms appear as a multiplicative term in Eq. (15) whereas in Eq. (24) the nonlinear terms appear as an addition to the linear Mathieu equation.

Although several mathematical techniques have been used to understand stability of nonlinear system [18,46], the discussion of stability in the papers cited above focus on the amplitude frequency response of the system. In the context of our present effort, we need to identify a method to obtain transition curves defined by $\beta_u = 0$ and 1 as well as *iso*-β_u lines for computing secular frequencies at different operating points. Based on our earlier experience, we investigated three techniques, which include the Lindstedt–Poincare, multiple scales and harmonic balance technique. The Lindstedt–Poincare and multiple scales are both asymptotic techniques, which provide periodic solutions to the nonlinear systems. The Lindstedt–Poincare technique is restricted to small perturbation parameters and thus low values of q and the multiple scales technique, used for study of transient dynamics, is more complicated. We preferred using the harmonic balance technique for its simplicity in obtaining a–q relations at $\beta_u = 0$ and 1 as well as for estimating *iso*-β_u lines within the stability plot for the nonlinear Mathieu equation. The problem of complicated algebra associated with inclusion of large number of terms in the harmonic balance analysis was circumvented by the use of commercial softwares MATLAB [47] and MAPLE [48]. In the paragraphs below, we report the method used in deriving the continuous fraction relationship similar to that generally used in the linear Mathieu equation, for estimating transition curves and *iso*-β_u lines.

In the method of harmonic balance the solution to Eq. (15) is written in terms of Fourier series with respect to time and has the form as given below

$$z = C + \sum_{n=-\infty}^{\infty} C_{2n} \cos(2n + \beta'_u)\frac{\Omega t}{2} \tag{25}$$

Here C is a constant and C_{2n} gives the amplitude of different harmonics that arises due to the nonlinearity; β'_u (the prime has been used to differentiate it from β_u which is traditionally used for linear equations) represents the frequencies of ion oscillation corresponding the values of (a_u, q_u) for the nonlinear Mathieu equation.

If we define $\omega_{u,n}$ as the angular frequency of order n for the motion of ions in the z and r direction, it is seen that the secular frequency in the axial and radial directions can be expressed from Eq. (25) as

$$\omega_{u,n} = (n + \tfrac{1}{2}\beta'_z)\Omega, \quad 0 \le n < \infty \tag{26}$$

and

$$\omega_{u,n} = -(n + \tfrac{1}{2}\beta'_z)\Omega, \quad -\infty < n < 0 \tag{27}$$

[7] and the secular frequency of the ion oscillation can be represented as

$$\omega_{z,0} = \tfrac{1}{2}\beta'_z\Omega \tag{28}$$

Substituting Eq. (25) in Eq. (15) and equating the constant and like terms to zero the following relations in the axial direction are obtained for $n = 0, 1, 2, 3, 4, \ldots$.

$$a_z C + \tfrac{1}{2} a_z \alpha_{2z} C_0 = 0 \tag{29}$$

$$-\beta_z'^2 C_0 + a_z C_0 + q_z C_2 + 2a_z \alpha_{2z} C C_0 + 2q_z \alpha_{2z} C C_2 + \tfrac{3}{4} a_z \alpha_{3z} C_0^3 + \tfrac{3}{4} q_z \alpha_{3z} C_2^3 = 0 \tag{30}$$

$$-(2+\beta_z')^2 C_2 + a_z C_2 + q_z C_0 + q_z C_4 + 2a_z \alpha_{2z} C C_2 + 2q_z \alpha_{2z} C C_0 + 2q_z \alpha_{2z} C C_4 + \tfrac{3}{4} a_z \alpha_{3z} C_2^3 + \tfrac{3}{4} q_z \alpha_{3z} C_0^3 + \tfrac{3}{4} q_z \alpha_{3z} C_4^3 = 0 \tag{31}$$

$$-(4+\beta_z')^2 C_4 + a_z C_4 + q_z C_2 + q_z C_6 + 2a_z \alpha_{2z} C C_4 + 2q_z \alpha_{2z} C C_2 + 2q_z \alpha_{2z} C C_6 + \tfrac{3}{4} a_z \alpha_{3z} C_4^3 + \tfrac{3}{4} q_z \alpha_{3z} C_2^3 + \tfrac{3}{4} q_z \alpha_{3z} C_6^3 = 0 \tag{32}$$

$$-(6+\beta_z')^2 C_6 + a_z C_6 + q_z C_4 + q_z C_8 + 2a_z \alpha_{2z} C C_6 + 2q_z \alpha_{2z} C C_4 + 2q_z \alpha_{2z} C C_8 + \tfrac{3}{4} a_z \alpha_{3z} C_6^3 + \tfrac{3}{4} q_z \alpha_{3z} C_4^3 + \tfrac{3}{4} q_z \alpha_{3z} C_8^3 = 0 \tag{33}$$

$$-(8+\beta_z')^2 C_8 + a_z C_8 + q_z C_6 + q_z C_{10} + 2a_z \alpha_{2z} C C_8 + 2q_z \alpha_{2z} C C_6 + 2q_z \alpha_{2z} C C_{10} + \tfrac{3}{4} a_z \alpha_{3z} C_8^3 + \tfrac{3}{4} q_z \alpha_{3z} C_6^3 + \tfrac{3}{4} q_z \alpha_{3z} C_{10}^3 = 0 \tag{34}$$

In Eqs. (29)–(34) we neglect appropriate higher order terms in the respective equations. From Eqs. (31) to (34) the generalized recursion relation solution for Eq. (15) can be written as follows

$$-(2n+\beta_z')^2 C_{2n} + a_z C_{2n} + q_z C_{2n-2} + q_z C_{2n+2} + 2a_z \alpha_{2z} C C_{2n} + 2q_z \alpha_{2z} C C_{2n-2} + 2q_z \alpha_{2z} C C_{2n+2} + \tfrac{3}{4} a_z \alpha_{3z} C_{2n}^3 + \tfrac{3}{4} q_z \alpha_{3z} C_{2n-2}^3 + \tfrac{3}{4} q_z \alpha_{3z} C_{2n+2}^3 = 0 \tag{35}$$

By collecting the terms having C_{2n} and C_{2n+2} coefficients from Eq. (35) we have

$$\frac{C_{2n}}{C_{2n+2}} = \frac{q_z(1 + 2\alpha_{2z} C + (3/4)\alpha_{3z} C_{2n+2}^2)}{(2n+\beta_z')^2 - a(1 + 2\alpha_{2z} C + (3/4)\alpha_{3z} C_{2n}^2) - q_z(1 + 2\alpha_{2z} C + (3/4)\alpha_{3z} C_{2n-2}^2)(C_{2n-2}/C_{2n})} \tag{36}$$

Similarly, by collecting C_{2n} and $C_{2n\text{-}2}$ from Eq. (35) it can be shown that

$$q_z \frac{C_{2n-2}}{C_{2n}} \left(1 + 2\alpha_{2z} C + \frac{3}{4}\alpha_{3z} C_{2n-2}^2\right) = (2n+\beta_z')^2 - a_z \left(1 + 2\alpha_{2z} C + \frac{3}{4}\alpha_{3z} C_{2n}^2\right) - q_z \left(1 + 2\alpha_{2z} C + \frac{3}{4}\alpha_{3z} C_{2n+2}^2\right) \frac{C_{2n+2}}{C_{2n}} \tag{37}$$

Now replacing n by $n-1$ in Eq. (36) we get

$$\frac{C_{2n-2}}{C_{2n}} = \frac{q_z(1 + 2\alpha_{2z} C + (3/4)\alpha_{3z} C_{2n}^2)}{(2n-2+\beta_z')^2 - a_z(1 + 2\alpha_{2z} C + (3/4)\alpha_{3z} C_{2n-2}^2) - q_z(1 + 2\alpha_{2z} C + (3/4)\alpha_{3z} C_{2n-4}^2)(C_{2n-4}/C_{2n-2})} \tag{38}$$

Substituting Eq. (38) in Eq. (37) and rearranging the terms, we have

$$(2n+\beta_z')^2 = a_z \left(1 + 2\alpha_{2z} C + \frac{3}{4}\alpha_{3z} C_{2n}^2\right) + q_z \left(1 + 2\alpha_{2z} C + \frac{3}{4}\alpha_{3z} C_{2n+2}^2\right)\left(\frac{C_{2n+2}}{C_{2n}}\right) + \frac{q_z^2(1 + 2\alpha_{2z} C + (3/4)\alpha_{3z} C_{2n-2}^2)(1 + 2\alpha_{2z} C + (3/4)\alpha_{3z} C_{2n}^2)}{(2n-2+\beta_z')^2 - a_z(1 + 2\alpha_{2z} C + (3/4)\alpha_{3z} C_{2n-2}^2) - q_z(1 + 2\alpha_{2z} C + (3/4)\alpha_{3z} C_{2n-4}^2)(C_{2n-4}/C_{2n-2})} \tag{39}$$

Eq. (39) represents a continuous fraction relationship between β_z, a_z and q_z in terms of C_{2n} coefficients. Expanding the Eq. (39) in terms of n and substituting $C = -a_{2z}C_0^2/2$ from Eq. (29) under the assumption $C_0 \gg C_{2n}$, for $n = 0$ we get

$$\begin{aligned}\beta_z'^2 = {} & a_z\left(1 - \alpha_{2z}^2 C_0^2 + \frac{3}{4}\alpha_{3z}C_0^2\right) \\ & + \cfrac{q_z^2(1-\alpha_{2z}^2C_0^2)^2}{(\beta_z'+2)^2 - a_z(1-\alpha_{2z}^2C_0^2) - \{q_z^2(1-\alpha_{2z}^2C_0^2)^2/ \\ \qquad [(\beta_z'+4)^2 - a_z(1-\alpha_{2z}^2C_0^2) - (q_z^2(1-\alpha_{2z}^2C_0^2)^2/(\beta_z'+6)^2 - a_z(1-\alpha_{2z}^2C_0^2) - \cdots)]\}} \\ & + \cfrac{q_z^2(1-\alpha_{2z}^2C_0^2 + (3/4)\alpha_{3z}C_0^2)(1-\alpha_{2z}^2C_0^2)}{(\beta_z'-2)^2 - a_z(1-\alpha_{2z}^2C_0^2) - \{q_z^2(1-\alpha_{2z}^2C_0^2)^2/ \\ \qquad [(\beta_z'-4)^2 - a_z(1-\alpha_{2z}^2C_0^2) - (q_z^2(1-\alpha_{2z}^2C_0^2)^2/(\beta_z'-6)^2 - a_z(1-\alpha_{2z}^2C_0^2) - \cdots)]\}}\end{aligned} \tag{40}$$

Similar analysis for the radial direction yields the following expression for β_r'

$$\begin{aligned}(\beta_r')^2 = {} & a_r\left(1 + \frac{3}{4}\alpha_{3r}C_0^2\right) + \cfrac{q_r^2}{(\beta_r'+2)^2 - a_r - \{q_r^2/(\beta_r'+4)^2 - a_r - [(q_r^2/(\beta_r'+6)^2 - a_r - \cdots)]\}} \\ & + \cfrac{q_r^2(1+(3/4)\alpha_{3r}C_0^2)}{(\beta_r'-2)^2 - a_r - \{q_r^2/(\beta_r'-4)^2 - a_r - [(q_r^2/(\beta_r'-6)^2 - a_r - \cdots)]\}}\end{aligned} \tag{41}$$

Eqs. (40) and (41) are similar to the continuous fraction relationship expression obtained for linear Mathieu equation with a few multiplicative terms that represent nonlinearities. Eq. (40) consists primarily of three terms, the first corresponding a and the second and the third being continuous fractions. It will be seen that all the a and q terms are multiplied by a term which are functions of nonlinearity as well as the amplitude of the fundamental frequency, C_0. It may be mentioned that this expression has been developed on the assumption that the amplitude of the frequency components other than the fundamental is negligible ($C_0 \gg C_{2n}$). Also, because of this assumption, only two of these three terms retain the influence of the octopole superposition whose contribution may be seen by the presence of α_{3z}. All the other a and q terms are multiplied by the factor $(1-\alpha_{2z}^2C_0^2)$, where α_{2z} corresponds to the weight of the hexapole term.

Eq. (41) is identical to Eq. (40) except for all terms related to hexapole superposition being zero on account of the absence of hexapole term in the equation of motion in the radial direction. Further, in view of the form of Eqs. (40) and (41), it is apparent that, like in the linear case, the stability curves $\beta_u' = 0$ starts at the origin. When all the nonlinearities are set to zero, as in an ideal Paul trap, this expression will become identical to the continuous fraction relation for linear Paul traps.

Eqs. (40) and (41) have been derived based on an approximations that the coefficients of higher order harmonics is zero (please see discussion after Eq. (39)). In order to check for the consequences that this approximation has on describing transition curves in nonlinear ion traps, we have compared the results predicted by Eq. (40) with numerical simulation of Eq. (15) along the $a_z = 0$ axis at $(q_z)_{\text{cut-off}}$. Numerical calculation is carried out by using fourth order Runge–Kutta method available in MATLAB [47]. The $(q_z)_{\text{cut-off}}$ value is determined by noting the value of q_z value at which the trajectories exceed the trap dimension (in our case it is $5e-3m$). In our computations, we have kept the step size as $1e-7$, initial velocity as zero and initial position as $1e-4m$.

Fig. 1 shows the shift of $(q_z)_{\text{cut-off}}$ for different values of nonlinearity (up to 5% hexapole + 5% positive octopole) obtained from our continuous fraction expression (Eq. (40)). This curve has been compared with the numerically obtained values for $(q_z)_{\text{cut-off}}$ for the same range of nonlinearity. From the plot it can

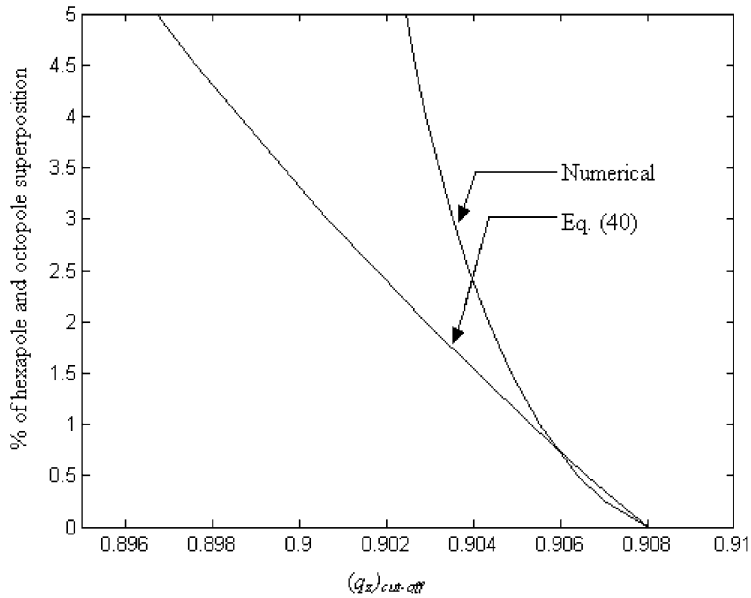

Fig. 1. Variation of $(q_z)_{\text{cut-off}}$ with weight of (hexapole + octopole) superposition.

be seen that for small values of hexapole and positive octopole superposition the $(q_z)_{\text{cut-off}}$ value calculated from Eq. (40) remains close to the $(q_z)_{\text{cut-off}}$ value calculated numerically. The difference between the $(q_z)_{\text{cut-off}}$ value estimated by Eq. (40) and the $(q_z)_{\text{cut-off}}$ value obtained numerically increases with increase in the hexapole and positive octopole superposition. For instance, the difference between the $(q_z)_{\text{cut-off}}$ value estimated by the Eq. (40) and the $(q_z)_{\text{cut-off}}$ value obtained numerically for 5% hexapole and 5% positive octopole superposition is about $5.7e-3$, with Eq. (40) predicting lower $(q_z)_{\text{cut-off}}$ value.

4. Results and discussions

The motivation of this paper is to understand the role of the hexapole and octopole field inhomogeneity in altering the stability region of ions as well as perturbing the *iso*-β_u lines within the Mathieu stability plot. In the paragraphs below, we present the results of our simulation for hexapole and octopole superposition of 2.5 or 5% and for value of $C_0 = z_0 = 4.9497e-3m$.

Figs. 2–5 show the shift in the transition curves corresponding to $\beta'_u = 0$ and 1 for different values of nonlinearity. The continuous fraction relationship given by Eq. (40) is used for computing the values of β'_z and the *iso*-β'_z lines are plotted in the a_z–q_z plane, where a_z and q_z are the Mathieu parameters for an ideal trapping conditions (i.e., no nonlinearity is present). Figs. 2–4 show the variation of the transition curves for 2.5 and 5% of hexapole superposition, 2.5 and 5% of positive octopole and 2.5 and 5% of negative octopole, respectively. Fig. 5 shows the shift in transition curves for 5% of hexapole superposition and 5% of positive octopole superposition. Stability boundaries corresponding to the ideal condition (when there is no nonlinearity) has also been included in all these plots for the sake of comparison. For plotting Figs. 6–9 we have considered only the axial direction and the dc potential is kept at zero (i.e., $a_z = 0$). Figs. 6 and 7 shows the variation of β'_z for different nonlinear conditions in axial direction. Fig. 6 shows the variation of β'_z with respect to q_z values for 5% hexapole superposition and Fig. 7 shows the variation in β'_z with respect to q_z for 5% positive octopole superposition and 5%

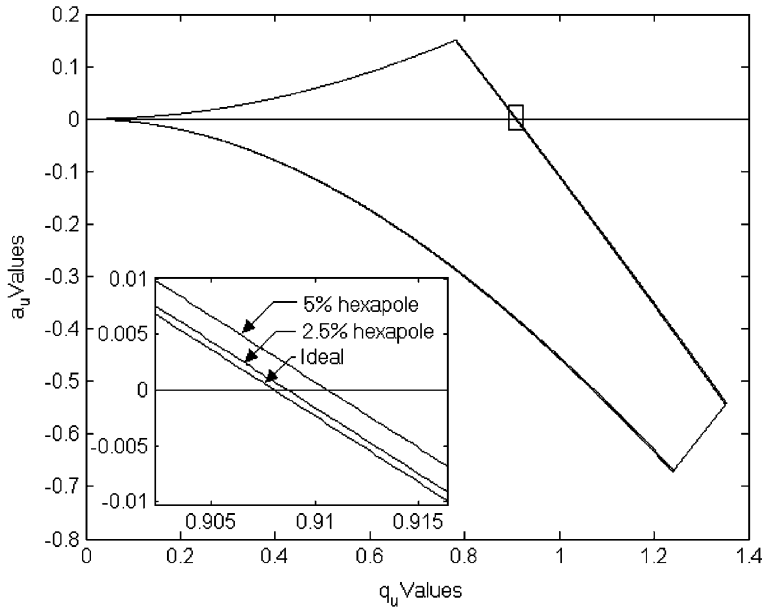

Fig. 2. Transition curves for 2.5 and 5% hexapole superposition.

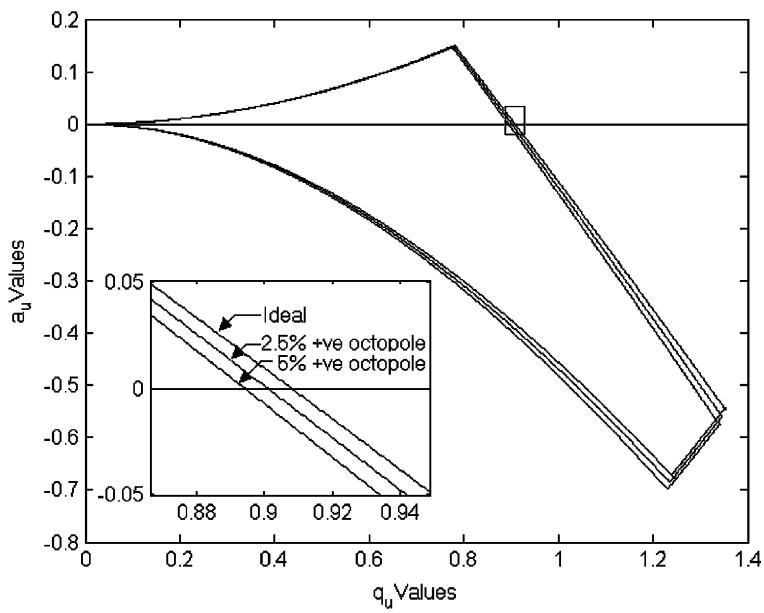

Fig. 3. Transition curves for 2.5 and 5% positive octopole superposition.

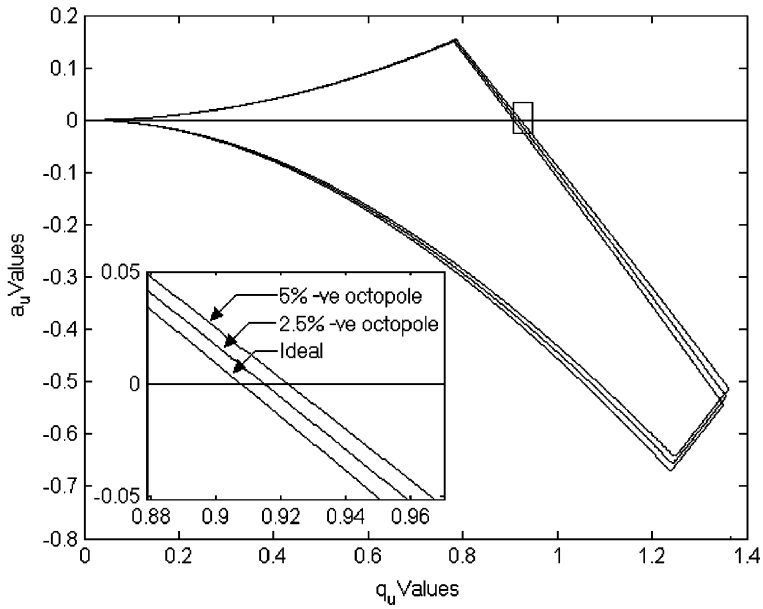

Fig. 4. Transition curves for 2.5 and 5% negative octopole superposition.

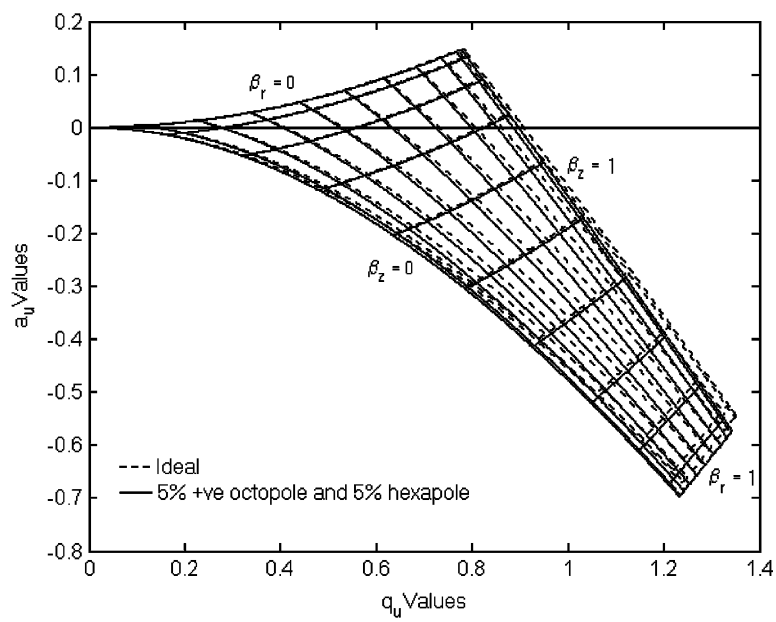

Fig. 5. Transition curves along with the *iso-β* lines for 5% positive octopole and 5% hexapole superposition.

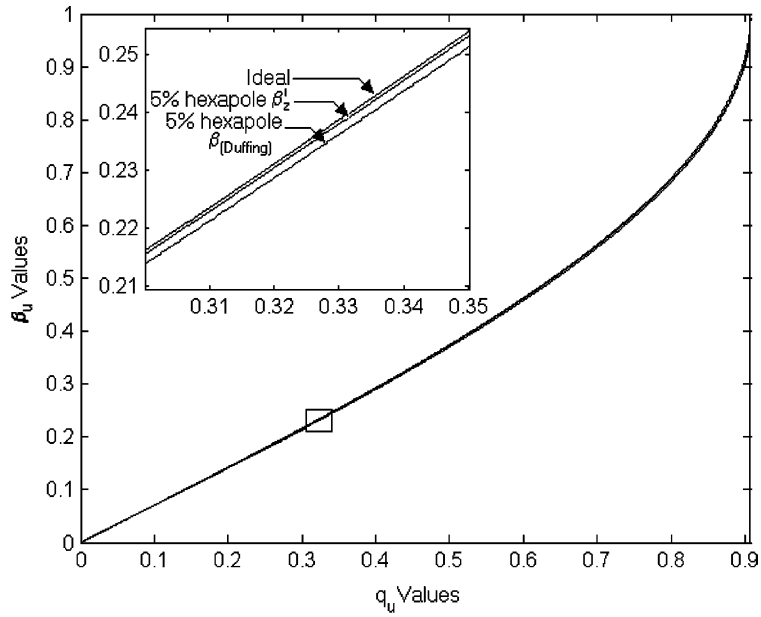

Fig. 6. Variation in β'_z and $\beta_{(\mathrm{Duffing})}$ with respect to q_z for 5% hexapole superposition.

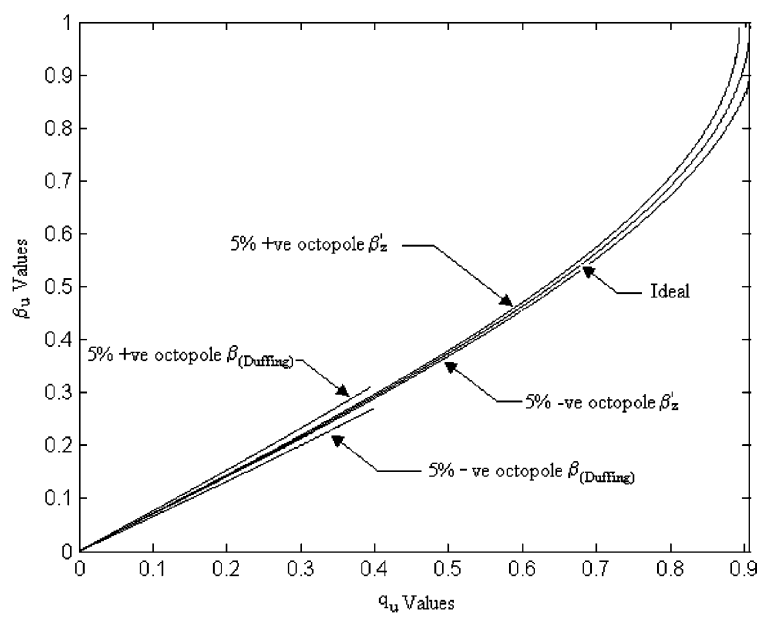

Fig. 7. Variation in β'_z and $\beta_{(\mathrm{Duffing})}$ with respect to q_z for 5% positive octopole and 5% negative octopole superposition.

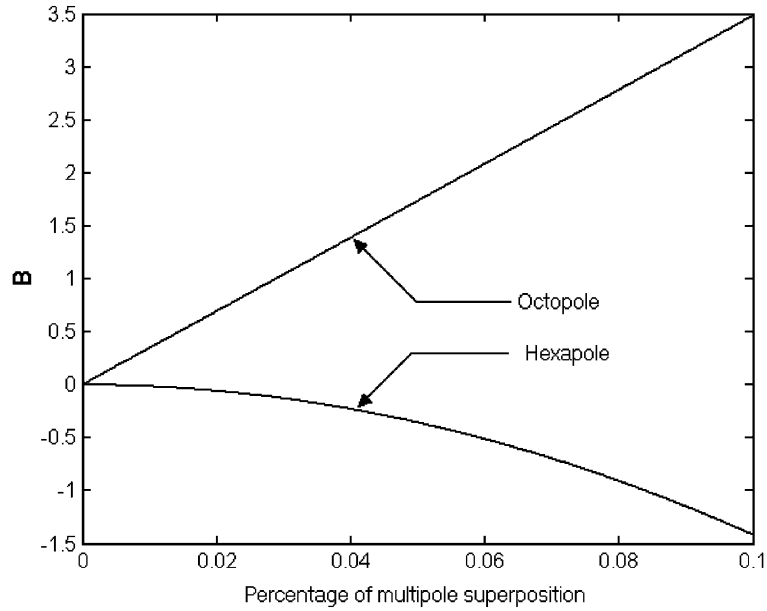

Fig. 8. Variation in B for different values of hexapole and octopole superposition.

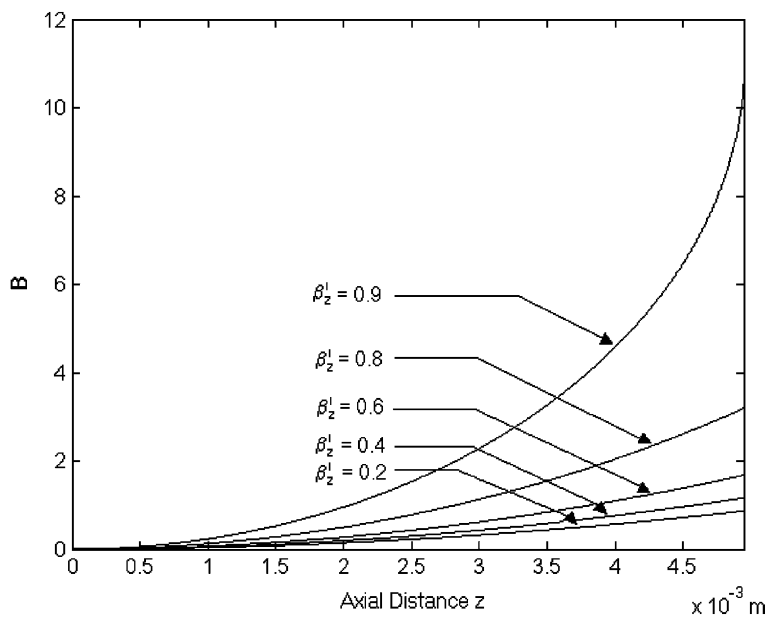

Fig. 9. Variation of B with respect to axial distance z for different values of β'_z.

negative octopole superposition. In Figs. 6 and 7, we have also included the curves for β_z values computed from continuous fraction relationship for the ideal trap and $\beta_{z(\text{Duffing})}$ values corresponding to Duffing equation approximation from our earlier publication [32], which is valid for $q_z < 0.4$, for the purpose of comparison.

For plotting Figs. 8 and 9 we introduce a new parameter B to represent the percentage of shift in β_z' value with respect to ideal β_z and is given by

$$B = \frac{\beta_z' - \beta_z}{\beta_z} \times 100 \tag{42}$$

Fig. 8 shows the variation of B for different values of hexapole and positive octopole superpositions when $\beta_z' = 0.5$. The changes in values of B with respect to axial distance z are shown in Fig. 9 for different values of β_z'.

Fig. 2 shows the transition curves in z and r direction in an a_z, q_z plane for 2.5 and 5% hexapole superposition. From Fig. 2 it is seen that for a particular a_z–q_z value the transition curve moves to the right of the stability boundary corresponding to the ideal Mathieu equation. This indicates that for a given (a_z, q_z) the β_z' value is less than the β_z value and occurs because the term corresponding to the hexapole superposition in Eq. (40) has a negative sign. Since the secular frequency is computed from Eq. (5), the hexapole superposition results in decrease in the secular frequency of the ion motion. This explains the decrease in secular frequency observed by Franzen [8] and Franzen et al. [14] in their numerical simulation studies. This results also matches with our earlier results [32,33] in which frequency perturbations are analyzed for $q_z < 0.4$ as well as the simulation results of Sudakov [35]. The inset shows a portion of the figure zoomed for better comparison with the ideal stability boundary. Two points are to be mentioned here. First is that there will be no shift in the transition curve in r direction as there is no term corresponding to hexapole superposition in the equation of ion motion (Eq. (20)). Secondly, the hexapole superposition varies the β_z' value quadratically and hence the shift in stability boundaries due to hexapole superposition is independent of the sign of superposition. This has been observed by authors in references [8,14,35] in their simulation studies.

Figs. 3 and 4 show the shifts of transition curves for octopole superpositions. Fig. 3 shows the effect of shift for 2.5 and 5% positive octopole superposition, whereas Fig. 4 shows the shift for 2.5 and 5% negative octopole superpositions. From Figs. 3 and 4, it is seen that the transition curve moves to the left of the stability boundary corresponding to the ideal Mathieu equation for a positive octopole superposition whereas it moves away to the right of the ideal Mathieu stability boundary for the negative octopole superposition. From the Figs. 3 and 4, it can be seen that the magnitude of the shift in transition curves due to the positive and negative octopole superposition are same but in opposite direction and hence the shifts are dependent on the sign of octopole superposition. Due to this shift and from Eq. (5) it is seen that the secular frequency of the ion oscillations will increase with increase in positive octopole superposition whereas it will decrease with increase in the negative octopole superposition. Cox et al. [21] in their experimental studies have also reported such behavior due to octopole superposition. Similar results have been reported by Franzen [8,13] and Franzen et al. [14] in their simulation studies. Makarov [15] and Luo et al. [16] have also pointed out the increase in secular frequency for positive octopole superposition in the cases when $q_z < 0.4$. These results are also in conformity with our earlier reports [32,33].

For a given trap with either positive or negative octopole superposition the shift in transition curves will be opposite in z and r directions as seen in Figs. 3 and 4. Positive octopole superposition will result in shifting the $\beta_z' = 0$ and 1 curves to the right of the ideal stability boundaries in z direction whereas it will shift the $\beta_z' = 0$ and 1 below the stability boundaries in r direction. This is due to the coefficient of octopole term in Eq. (15), α_{3z}, having a positive sign whereas the co-efficient of octopole term in Eq. (20), α_{3r}, has a negative sign. Alheit et al. [49] in their experimental observations of instabilities in a Paul trap with higher order anharmonicities have shown a similar effect in variation of β_z and β_r with respect to octopole

superposition. Comparing Figs. 2 and 4 it can be seen that hexapole and negative octopole have the same effect of shifting the stability boundaries to higher values of q_z. However, the magnitude of shift will be larger for a given negative octopole superposition in comparison to same value of hexapole superposition.

Fig. 5 shows the stability diagram for 5% hexapole and 5% positive octopole superposition with the *iso*-β lines included in the figure. In this plot, the broken lines corresponds to the stability boundary and *iso*-β_z for an ideal condition while the solid lines represents the transition curves and *iso*-β'_z for the given nonlinear condition. This plot is similar to that of the experimental stability plot obtained by Johnson et al. [11] in their studies on the stretched quadrupole trap although they attributed the shift to different factors such as scan function and the effective time of the applied voltages in their experimental setup. Arkin et al. [12] in their experimental studies to characterize a hybrid trap also obtained a distorted stability plot similar to that of Fig. 5. The hybrid trap used by Arkin et al. [12] can be considered as a highly distorted nonlinear Paul trap and consequently, can be interpreted to result from superposition of positive octopole.

Fig. 6 plots variation of β'_z with respect to q_z values for 5% hexapole superposition. This plot compares β_z values computed from our earlier paper [32] to our present studies. Our earlier study was based on pseudopotential well approximation and the equation of ion motion was represented by Duffing equation with the validity of q_z up to 0.4. The value of $\beta_{z\,(\mathrm{Duffing})}$ is calculated with the help of the following equation

$$\beta_{z(\mathrm{Duffing})} = \frac{2\omega}{\Omega} \tag{43}$$

where ω is the shifted secular frequency for a given hexapole and octopole superposition and is given by [32]

$$\omega = \omega_0 \left(1 + \frac{144f - 405h^2}{48} A_0^2\right) \tag{44}$$

Here ω_0 is the ideal secular frequency and A_0 is the amplitude of ion oscillation, which in our present computation has been fixed as z_0 (the shortest distance from the center of the trap to one endcap electrode) with the value of $4.9497e - 3m$ (for a ring electrode radius of $7e - 3m$). From the figure it is seen that both β'_z and $\beta_{z\,(\mathrm{Duffing})}$ deviates from the β_z values computed for an ideal trap for a given hexapole superposition with $\beta_{z\,(\mathrm{Duffing})}$ having a larger deviation from β_z compared to β'_z.

Fig. 7 shows variation of β'_z and $\beta_{z\,(\mathrm{Duffing})}$ with respect to q_z for 5% positive octopole and 5% negative octopole superposition along the $a_z = 0$ axis. Here too $\beta_{z\,(\mathrm{Duffing})}$ has a larger deviation from β_z than β'_z. β'_z increases for a positive octopole superposition and decreases for a negative octopole superposition in comparison to β_z and both curves display an increasing trend with increase in q_z values. Cai et al. [36] and Alheit et al. [49] have observed similar behavior in their experimental studies.

Fig. 8 shows the variation in B (Eq. (42)) for different hexapole and octopole superposition. In this plot the value of q_z is kept at 0.6393, corresponding to a β_z value of 0.5. It is seen that B increases linearly with positive octopole superposition and decreases quadratically with hexapole superposition in conformity with the expectation of linear increase in secular frequency for positive octopole superposition and a quadratic decrease in the secular frequency for hexapole superposition. These observations are on account of α_{2z}, corresponding to the hexapole superposition, appearing as a quadratic term and α_{3z}, corresponding to the octopole superposition, varying linearly in Eq. (15). The magnitude of variation of β'_z with the negative octopole is similar to that of the positive octopole superposition but the direction of shift will be opposite. Similar results have been reported by Franzen et al. [8,14].

Fig. 9 shows the variation of B with respect to the axial distance z from the center of the trap for 5% hexapole and 5% positive octopole superposition for β'_z values of 0.2, 0.4, 0.6, 0.8 and 0.9. From the figure it is seen that at the center of the trap the value for B is zero indicating that the field at the center is due to pure quadrupolar potential. From the figure the quadratic variation of B with respect to axial distance is evident from the curves for higher β'_z values. Similar results have been reported by Franzen [8,13] and Franzen

et al. [14] in their simulation studies. Splendore et al. [50] also have reported such behavior in their simulation study of kinetic energies during resonant excitation in a stretched ion trap. This figure also shows that the shift becomes more pronounced as $\beta_z' \rightarrow 1$.

5. Concluding remarks

The motivation of the present study was understand the role of field inhomogeneties in altering the stable regions of nonlinear Paul trap operation. We have sought to define the boundaries of the stability regions by means of transition curves, which correspond to the periodic solution of a weakly nonlinear Mathieu equation. The harmonic balance technique was employed to develop a continuous fraction expression for β_u in terms of a_u and q_u.

Although these transition curves developed here cannot strictly be considered as the stability boundaries of the nonlinear Mathieu equation, it was seen that they adequately reflect experimental observations available in literature for stability of ions in nonlinear Paul traps. The shift in the transition curves from the ideal stability boundaries varies quadratically with hexapole superposition and is sign insensitive whereas for octopole superposition it varies linearly and is sign sensitive. For the same value of superposition, the shift in the transition curves is larger for negative octopole superposition than for hexapole superposition. The shift in transition curves from the ideal stability boundaries increase with increase in q_u values. These predictions obtained from our expressions are in qualitative agreement with experimental observations in literature.

Secular frequency shifts obtained by our continuous fraction expression have been compared with both experimental work as well as simulation studies reported in literature. It is seen that the shift in secular frequency varies quadratically with hexapole superposition and is independent on the sign of superposition. Similarly, our analytical expression suggests that the secular frequency varies linearly with octopole superposition and is dependent on the sign of superposition. For a given hexapole or octopole superposition the shift in secular frequency increases with increase in q_z values.

Acknowledgements

We are grateful to Dr. Anindya Chatterjee, Department of Mechanical Engineering of our Institute for his critical comments and suggestions on the manuscript. We would also like to thank two anonymous reviewers for their insightful comments.

References

[1] P.H. Dawson, Quadrupole Mass Spectrometry and Its Application, Elsevier, Amsterdam, 1976.
[2] R.D. Knight, Int. J. Mass Spectrom. Ion. Phys. 51 (1983) 127.
[3] R.E. March, R.J. Hughes, Quadrupole Storage Mass Spectrometry, Wiley/Interscience, New York, 1989.
[4] R.E. March, Int. J. Mass Spectrom. Ion Process. 118/119 (1992) 72.
[5] N.W. McLachlan, Ordinary Non-linear Differential Equations in Engineering and Physical Sciences, Oxford University Press, Oxford, 1958.
[6] M. Abromowitz, I.A. Stegun, Handbook of Mathematical Functions, Dover Publications Inc., New York, 1970.
[7] R.E. March, Frank A. Londry, in: R.E. March, J.F.J. Todd (Eds.), Practical Aspects of Ion Trap Mass Spectrometry, CRC Press, New York, 1995, Chapter 2, p. 25.
[8] J. Franzen, Int. J. Mass Spectrom. Ion Process. 125 (1993) 165.
[9] E. Fischer, Z. Phys. 156 (1959) 1.
[10] J.E. Fulford, D.-N. Hoa, R.J. Hughes, R.E. March, R.F. Bonner, G.J. Wong, J. Vac. Sci. Technol. 17 (1980) 829.
[11] J.V. Johnson, R.E. Pedder, R.A. Yost, Rapid Comm. Mass Spectrom. 6 (1992) 760.
[12] C.R. Arkin, B. Goolsby, D.A. Laude, Int. J. Mass Spectrom. 190/191 (1999) 47.
[13] J. Franzen, Int. J. Mass Spectrom. Ion Process. 106 (1991) 63.
[14] J. Franzen, R.H. Gabling, M. Schubert, Y. Wang, in: R.E. March, J.F.J. Todd (Eds.), Practical Aspects of Ion Trap Mass Spectrometry, CRC Press, New York, 1995, Chapter 3, p. 49.
[15] A.A. Makarov, Anal. Chem. 68 (1996) 4257.
[16] X. Luo, X. Zhu, K. Gao, J. Li, M. Yan, L. Shi, et al., Appl. Phys. B 62 (1996) 421.
[17] K.O. Friedrichs, J.J. Stoker, Quart. Appl. Math. 1 (1943) 97.
[18] A.H. Nayfeh, D.T. Mook, Nonlinear Oscillations, Wiley/Interscience, New York, 1979.
[19] R.G. Frehlich, S. Novak, Int. J. Non-Linear Mech. 20 (1985) 123.
[20] K. Sugiyama, J. Yoda, Appl. Phys. B 51 (1990) 146.

[21] K.A. Cox, C.D. Cleven, R.G. Cooks, Int. J. Mass Spectrom. Ion Process. 144 (1995) 47.
[22] M. Nappi, V. Frankevich, M. Soni, R.G. Cooks, Int. J. Mass Spectrom. Ion Process. 177 (1998) 91.
[23] J. Louris, J. Schwartz, G. Stanfford, J. Syka, D. Taylor, in: Proceedings of the 40th ASMS Conference on Mass Spectrometry and Allied Topics, Washington, DC, 1992, p. 1003.
[24] F. Vedel, M. Vedel, in: R.E. March, J.F.J. Todd (Eds.), Practical Aspects of Ion Trap Mass Spectrometry, CRC Press, New York, 1995, Chapter 8, p. 346.
[25] K. Sugiyama, J. Yoda, Appl. Phys. B 51 (1990) 146.
[26] R.E. March, A.W. McMahon, F.A. Londry, R.L. Alfred, J.F.J. Todd, F. Vedel, Int. J. Mass Spectrom. Ion Process. 95 (1989) 119.
[27] R.E. March, A.W. McMahon, E.T. Allinson, F.A. Londry, R.L. Alfred, J.F.J. Todd, et al., Int. J. Mass Spectrom. Ion Process. 99 (1990) 109.
[28] F.A. Londry, R.L. Alfered, R.E. March, J. Am. Soc. Mass Spectrom. 4 (1993) 687.
[29] H.A. Bui, R.G. Cooks, J. Mass Spectrom. 33 (1998) 297.
[30] D.A. Dahl, Int. J. Mass Spectrom. 200 (2000) 3.
[31] M. Vedel, J. Rocher, M. Knoop, F. Vedel, Appl. Phys. B 66 (1998) 191.
[32] S. Sevugarajan, A.G. Menon, Int. J. Mass Spectrom. 189 (1999) 53.
[33] S. Sevugarajan, A.G. Menon, Int. J. Mass Spectrom. 197 (2000) 263.
[34] S. Sevugarajan, A.G. Menon, Int. J. Mass Spectrom. 209 (2001) 209.
[35] M. Sudakov, Int. J. Mass Spectrom. 206 (2001) 27.
[36] Y. Cai, W.P. Peng, S.J. Kuo, H.C. Chang, Int. J. Mass Spectrom. 214 (2002) 63.
[37] N.C. Rana, P.S. Joag, Classical Mechanics, McGraw-Hill, New Delhi, 2000.
[38] Y. Wang, J. Franzen, K.P. Wanczek, Int. J. Mass Spectrom. Ion Process. 124 (1993) 125.
[39] E.C. Beaty, Phys. Rev. A 33 (1986) 3645.
[40] L.S. Brown, G. Gabrielse, Rev. Mod. Phys. 58 (1986) 233.
[41] N.W. McLachlan, Ordinary Non-linear Differential Equations in Engineering and Physical Sciences, Oxford University Press, Oxford, 1958.
[42] G.M. Mahmoud, Int. J. Non-Linear Mech. 32 (1997) 1177.
[43] D.Y. Hsieh, J. Math. Phys. 21 (1980) 722.
[44] L.D. Zavodney, A.H. Nayfeh, J. Sound Vibration 120 (1988) 63.
[45] S. Natsiavas, S. Theodossiades, I. Goudas, Int. J. Non-Linear Mech. 35 (2000) 53.
[46] A.H. Nayfeh, Perturbation Methods, Wiley/Interscience, New York, 1973.
[47] MATLAB Reference Guide, The Math Works, Inc., US, 1992.
[48] K.M. Heal, M.L. Hansen, K.M. Rickard, MAPLE 6.0, Learning Guide, Waterloo Maple Inc., Canada, 2000.
[49] R. Alheit, C. Hennig, R. Morgenstern, F. Vedel, G. Werth, Appl. Phys. B 61 (1995) 277.
[50] M. Splendore, F.A. Londry, R.E. March, R.J.S. Morrison, P. Perrier, J. Andre, Int. J. Mass Spectrom. Ion Process. 156 (1996) 11.